The ParB-CTP Cycle Activates Phase Separation in Bacterial DNA Segregation

Linda Delimi[1], Perrine Revoil[2], Jérôme Rech[2], Jean-Yves Bouet[2,*], Jean-Charles Walter[1,*]

[1]Laboratoire Charles Coulomb (L2C), Univ. Montpellier, CNRS, Montpellier, France
[2]Laboratoire de Microbiologie et de Génétique Moléculaires (LMGM), CBI, CNRS, Univ. Toulouse, UPS, Toulouse, France

* jean-yves.bouet@univ-tlse3.fr
* jean-charles.walter@umontpellier.fr
* corresponding authors with equal contribution

Abstract

Cell function relies on liquid-like organelles formed through phase transitions, yet the mechanisms ensuring their specificity and rapid assembly remain poorly understood. In bacterial chromosome segregation via the ParABS system, hundreds of ParB proteins are recruited around the centromere-like *parS* sequence forming the partition complex. Recent studies have shown that ParB binds CTP and undergoes cycles of binding and unbinding near *parS*, however, this accounts for the recruitment of only a small fraction of ParB molecules, leaving its role unclear. Separately, a lattice gas model with fixed interaction energy has been proposed to describe ParB phase separation, but it fails to explain key experimental observations, including the absence of droplets in ParB variants. We reconcile these two perspectives by proposing that the ParB-CTP cycle acts as a molecular switch that enhances ParB-ParB interactions, triggering phase transition from vapor to liquid-like condensates. Our hypothesis is supported by numerical simulations of droplet formation and experiments showing that ParB variants disrupting the CTP cycle fail to undergo phase separation. These findings establish a mechanistic framework for ParB-CTP-mediated phase transitions and may have broader implications for understanding the spatial control of intracellular condensate formation.

Introduction

The formation of membraneless compartments with high concentrations of proteins, also called organelles, relies on the physical mechanism of phase separation [1]. The resulting compartments consist of droplet-like objects that share liquid properties. It is an efficient way to quickly recruit, with a small amount of energy, a population of proteins to, for example, catalyze a chemical reaction. A prominent early example of phase separation is the assembly of P granules in *C. elegans* [2]. These condensates were among the first to show how weak, multivalent interactions facilitate the rapid and selective organization of biomolecules [1]. Similarly, in bacteria, several phase-separating systems exhibit liquid-like properties, such as in RNA processing regulation (BR-bodies) and the initiation of cell division (FtsZ-SlmA) [3]. Despite these insights, mechanisms leading to highly controlled phase transitions are still not well understood.

Bacterial DNA segregation offers a system for investigating the onset of droplet formation *in vivo*. Faithful DNA segregation is an essential biological process to ensure that each offspring receives at least one copy of each replicon, chromosome or plasmid. The ParAB*S* systems are the main active DNA partitioning systems used by bacterial chromosomes and most low-copy-number plasmids [4]. It consists of ParA, a Walker-type ATPase, and ParB, a CTPase that binds to *parS* centromere sites with high affinity. The initial step is the binding of a few ParB onto *parS* triggering the recruitment of hundreds of ParB proteins around *parS*, *i.e.*, most of the intracellular ParB population ($> 90\%$) [5]. These large nucleoprotein complexes are called partition complexes. ParA mediates their separation by activating its ATPase activity, which is catalyzed by the high local concentration of ParB [6, 7].

The partition complexes display several liquid-like properties *in vivo*, including: the averaged spherical shape of the condensate, which minimizes the surface tension, the ability of ParB foci to fuse, the intracellular mobility of ParB, which is $\sim$100 times slower within ParB complexes compared to the surrounding diluted phase, the rapid exchange of ParB between distinct partition complexes, occurring within a few minutes [8–10]. Furthermore, *in vitro* studies have demonstrated the self-organization of ParB into droplets [11].

The lattice gas (LG) is a paradigmatic model for phase transitions where nearest-neighbour particles display attractive interaction. The LG exhibits two distinct phases: a vapor phase, where particles are randomly distributed within the volume, and a liquid-vapor (LV) coexistence phase, where the liquid coexists with a residual vapor phase. Within the LV phase, a metastable and a stable region can be identified. We previously investigated the partition complex formation, using this model at fixed ParB-ParB interaction energy in the metastable region. However, within this framework, the timescale of the complex formation is

orders of magnitude larger than the cell cycle, making it biologically irrelevant [10].

New critical insight into this process is provided via ParB binding to CTP, and the subsequent ParB-CTP cycle, as recently described by the Clamping & Sliding (CS) mechanism [12]. The CS model involves a sequential multi-step process: (i) the specific binding of ParB to *parS*, a 16-bp DNA motif [13–15], (ii) the binding of CTP to *parS*-bound ParB [16, 17], followed by (iii) the conversion of ParB into a clamp and its ejection from *parS* due to steric clash upon ParB remodeling [17], (iv) the subsequent diffusion over *parS*-proximal DNA [17], and lastly (v) the unloading of ParB after the clamp reopens [18].

The CS model was proposed to explain the recruitment of most intracellular ParB to DNA [9, 19]. However, our findings reveal that CS alone can only account for a small fraction of ParB onto DNA (< 10 ParB proteins) and the observed loading and unloading timescales are inconsistent with experiments [10, 12]. New evidence from both *in vitro* experiments and simulations indicates that recruitment events can occur in *trans* but are generally sparse [19, 20]. Importantly, the binding of ParB to both *parS* and CTP is essential for complex formation. In the absence of *parS*, or when ParB variants lack CTP-binding ability, partition complexes fail to form [5, 9, 21, 22]. Additionally, the CTPase activity of ParB facilitates the release of clamped ParB from *parS*-proximal DNA [9, 11, 23]. Despite these findings, the functional role of CTP binding remains unclear and is still under debate.

To reconcile the LG and CS mechanisms, we hypothesize that the ParB-CTP cycle activates the phase transition by enhancing ParB-ParB interactions, providing a regulatory mechanism to fine-tune the formation and stability of partition complexes. In the section 1, we outline this hypothesis and describe the theoretical basis of our model that couples LG framework with the CS mechanism. In the section 2, we present kinetic simulations of partition complex formation, demonstrating that phase separation depends on an activation in order to occur in a biologically relevant timescale. In the section 3, we provide experimental evidence showing that modifications of the ParB-CTP cycle impair partition complex formation. We employed the well-characterized ParAB*S* system of plasmid F, hereafter called ParABS_{F} [24]. Specifically, we engineered ParB$_{\mathrm{F}}$ variants in the CTP binding and hydrolysis motifs, both of which exhibited loss of the ParB$_{\mathrm{F}}$ droplet formation. We conclude by discussing the implications of these findings for understanding ParB-mediated DNA segregation.

1 Lattice Gas coupled to CTP activation of ParB

In this section, we present a two-step model combining a phase separation and a CTP activation during the CS cycle. We show a schematic representation of the ParB-DNA complex in Fig. 1A, showcasing the macroscopic behaviors of ParB observed experimentally. We define by J the interaction energy between ParB. On top of the panel, in the absence of *parS* or for ParB variants displaying modification of the ParB-CTP cycle, no droplets are observed [5, 9, 11, 21, 22]. ParB are then represented by green dots and feature an interaction energy J_{V}. The bottom of the panel depicts the wild type (WT) scenario, where activated ParBs (magenta dots, interaction energy J_{LV}) form droplets around *parS* sites. In the latter case, a majority of ParB proteins ($\sim$95%) forms a dense complex in equilibrium with a small fraction ($\sim$5%) outside [10]. These observations led to the development of the LG model to account for those macroscopic behaviors, thus enhancing the role of molecular ParB interactions. We define the LG model, previously proposed to describe the liquid-like behavior of ParB condensates [10]. The Hamiltonian of the LG model . Autre point mineur, j'ai l'impression que la Fig.S5 n'est pas utilisée. Merci de confirmer sinon on la supprime. JCis:

$$\mathcal{H} = -J \sum_{\langle i,j \rangle} \phi_i \phi_j + \sum_i \epsilon_i \phi_i \,, \tag{1}$$

where J represents the contact interaction energy, ϕ_i is the occupation variable of the lattice site i (ϕ_i =0 or 1 if the site is empty or occupied, respectively) and $\langle i, j \rangle$ denotes pairs of nearest neighbors. The interaction energy ϵ_i of the site i is defined by $\epsilon_i = \epsilon_{\mathrm{s}} - \epsilon_{\mathrm{ns}}$, the difference between the affinity of ParB on specific DNA at *parS* (ϵ_{s}) and non-specific DNA (nsDNA, ϵ_{ns}). The lattice serves as a mean field representation of indistinguishable DNA, including both chromosomal and plasmid DNA, present stochastically in the vicinity of *parS* since the plasmid is embedded in the nucleoid [26].

Fig. 1B, presents the LG phase diagram in the $(1/(\beta J),\ \rho)$ plane where $\beta = 1/(kT)$ is the inverse temperature, k the Boltzmann constant, T the absolute temperature and ρ the density. It is obtained in the mean field approach [25], yet it is a reasonable approximation to sketch the phenomenology of the realistic three dimensional LG. In this case, no exact solution exists and it requires thus to be studied numerically. At low interaction energy, J_{V}, the system remains in a vapor-like state (green), unable to form droplets. For sufficiently high interaction energy J_{LV}, the system is set in the LV phase (purple) below the coexistence line (full black line). At the coexistence line, the LG displays a first order (or discontinuous) transition. The LV phase is characterized by the existence of liquid droplet formation and consists of two regions: (i) the metastable region (white and magenta stripes), located between the coexistence and the spinodal line (black dashed line) and (ii) the stable region, below the spinodal line. The difference between these two regions lies in kinetic effects. For completeness, we notice the existence of a critical point at $\rho = 1/2$ and

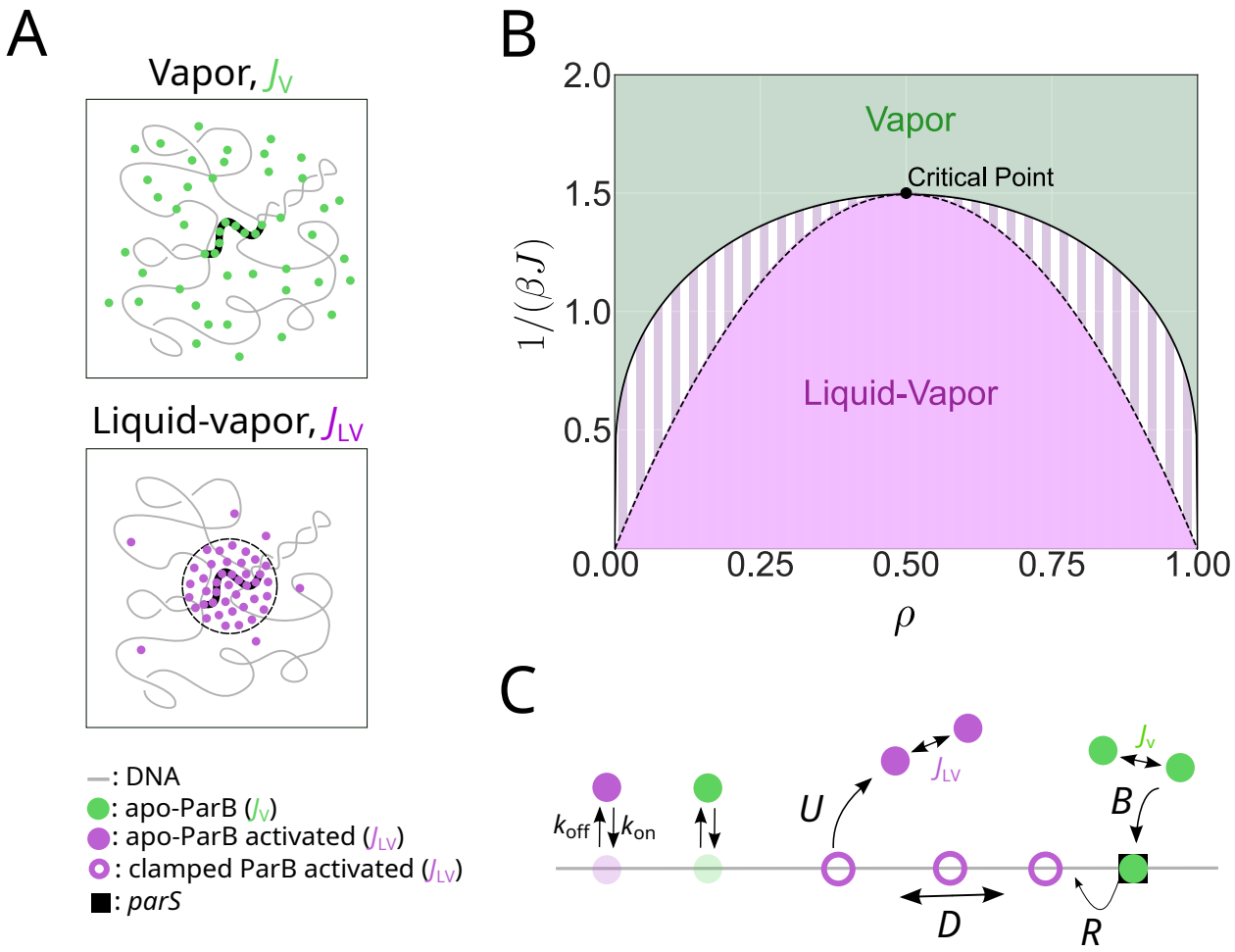

Figure 1. *Modeling of phase transition controlled by ParB-CTP cycle activation.* **A** Illustration of the ParB-DNA complex macroscopic behaviors. (top) Mutants with ParB variants disrupting ParB-CTP cycle fail to form complexes (ParB as green dots, with interacting energy J_V). (bottom) WT cells display liquid-like ParB droplets around *parS*, with activated ParB (magenta dot, with interacting energy J_{LV}). **B** Phase diagram of a LG in the $(1/(\beta J), \rho)$ plane (mean-field solution [25]). The coexistence line (solid line) separates the vapor (green) from the liquid-vapor (purple) phase. The spinodal line (dashed line) demarcates the metastable region (white and magenta stripes) within the LV phase. **C** Schematic representation of ParB activation in the Clamping & Sliding stage. Apo-ParB specifically binds to *parS* (black square) at the rate B, which increases ParB affinity for CTP. CTP-binding induces a conformational change converting ParB-CTP into a clamp (magenta circle) over the DNA, leading to its ejection from *parS* at the rate R. For simplicity we hypothesize that the activation takes place between this latter step and the unbinding from DNA. Clamped ParB-CTP can diffuse along the DNA, with a diffusion coefficient D, until being unloaded from non-specific-DNA (nsDNA) through clamp opening at the rate U, returning to its apo form (magenta dot). All forms of apoParB can bind and unbind to nsDNA with rates k_{on} and k_{off}, resp.

$T = T_c$ ($T_c = 3/2$ in the mean field case), at which LG model undergoes a continuous (or second-order) phase transition.

The CS model, as depicted in Fig. 1C, involves the specific binding of apoParB (green dots) to *parS* sites (black square) at the binding rate B. This step is not rate-limiting due to the high affinity of ParB for *parS* (in the nanomolar range [6]) and its higher rate compared to other steps, as recapitulated in Ref. [12]. Binding to *parS* increases the affinity of ParB for CTP [16, 17]. Upon CTP binding, ParB undergoes a conformational change, forming a clamp-like structure (magenta circle) that sterically clashes with the DNA double helix, leading to ParB release from *parS* [9, 23]. The combined rates of CTP binding and subsequent ParB release are modeled with a single rate R (release rate), as the latter is the limiting step [12]. Once released, the clamped-ParB diffuses along the DNA (grey line) at the diffusion rate D. Lastly, upon CTP release, either through unbinding or hydrolysis, ParB returns to its apo-form (magenta dots), which triggers unclamping and subsequent unloading from nsDNA at a rate U.

The novelty and main hypothesis of the present study is that ParB undergoes an activation switch from an inactive (green) to an active (magenta) form, with enhanced ParB-ParB interaction energy transitioning from J_{V} to J_{LV} (activated), where $J_{\mathrm{LV}} > J_{\mathrm{V}}$. We propose that this switch occurs specifically between the release of ParB from *parS* and its unloading from nsDNA. Note that both forms of ParB can bind to nsDNA, independently of the CS mechanism, with respective binding and unbinding rates k_{on} and k_{off}.

The following section investigates numerically the type of activation necessary to trigger the phase transition in a biologically relevant timescale. To this end, we assay ParB macroscopic behavior with MC simulations and analyze the kinetics of droplet formation under activation in the LV phase.

2 ParB droplet formation requires an activation of ParB-ParB interactions

According to the LG model, droplet formation is restricted to the LV phase. The question remains whether activation occurs within a biologically relevant timescale.

To address this, we conducted numerical simulations to study the kinetics of droplet formation. Our simulations were performed on a cubic lattice of size $400 \times 100 \times 100$, where the lattice unit corresponds to the size of a ParB binding site, 16 bp of DNA [13–15]. The simulations were performed in the canonical ensemble, maintaining a fixed number of particles N_b to approximate the regulated number of intracellular ParB proteins (here $N_b = 300$). Note that the density is low ($\rho \sim 10^{-4}$) and we expect thus a first order transition, see Fig. 1B. The order parameter ψ is defined as the average density of bonds per particle:

$$\psi = \frac{1}{N_b} \sum_{\langle i,j \rangle} \phi_i \phi_j \,. \tag{2}$$

It distinguishes the vapor phase ($\psi \approx 0$) from the LV phase ($\psi \approx q$), where q is the coordination number of the lattice. The equilibrium phase diagram of the LG corresponding to biological parameters is shown in Fig. 2A, where ψ is plotted as a function of the interaction energy J. Note that J is expressed in unit of kT. The red (increasing J) and blue (decreasing J) curves exhibit a hysteresis cycle, characteristic of a first-order phase transition. This defines three regimes: vapor ($J < 2.7$), metastable LV ($2.7 < J < 3.1$), and stable LV ($J > 3.1$). In brief, J was incremented (red curve) or decreased (blue curve) in discrete steps ($\Delta J = 0.06$, see Supp. Methods for more details). We observe a first order transition at biological values of $J \approx 3$. An activation from the vapor to the LV phase would correspond to a reasonable increase of J, by an increment of a few times the thermal energy.

In Fig. 2B, we plot the time evolution of ψ in order to study the out-of-equilibrium behavior of the droplet formation. Our protocol consists in preparing the system in a completely disordered state (vapor phase with $J = 0$) and let it evolve after activation in the LV phase ($J = 4.7$). This can also be interpreted as a quench, as increasing the coupling theoretically corresponds to decreasing the temperature. Under the experimental conditions described in the section 3, the cell cycle is approximately 60 minutes or 3.5×10^3s, see [8]. Since one MC iteration approximates one second, the total simulation time of 10^4s corresponds to about ten times the cell cycle. The purple curve describes the evolution of ψ when the LG is activated into the LV phase ($J = 4.7$). The droplet formation (defined as the time when ψ reaches half of its equilibrium value) occurs in average in $3{\times}10^3$s corresponding to $\approx$45 minutes, based on 10^3 simulations. Despite the simplicity of our approach and the most unfavorable initial conditions (ParB randomly distributed inside the cell instead of being clustered near *parS* because of the ParB operon close to *parS*), droplet formation occurs within a timescale corresponding to a fraction of the cell cycle. The green curve describes the evolution of ψ when the LG remains in the vapor phase ($J = 2.5$). No complex formation is observed, as it is the case in the absence of *parS* or certain ParB variants. As a control simulation, the grey dashed curve represents a quench into the metastable region ($J = 3$). Notably, green and grey curves are indistinguishable, with no nucleation observed within ten times the cell cycle, in agreement with Ref. [10]. This supports that neither an activation of the interaction energy nor a fixed interaction within the metastable region is sufficient for complex formation.

These simulations support the hypothesis that ParB must undergo an activation of its interaction energy to reproduce the observed experimental phenomenology:

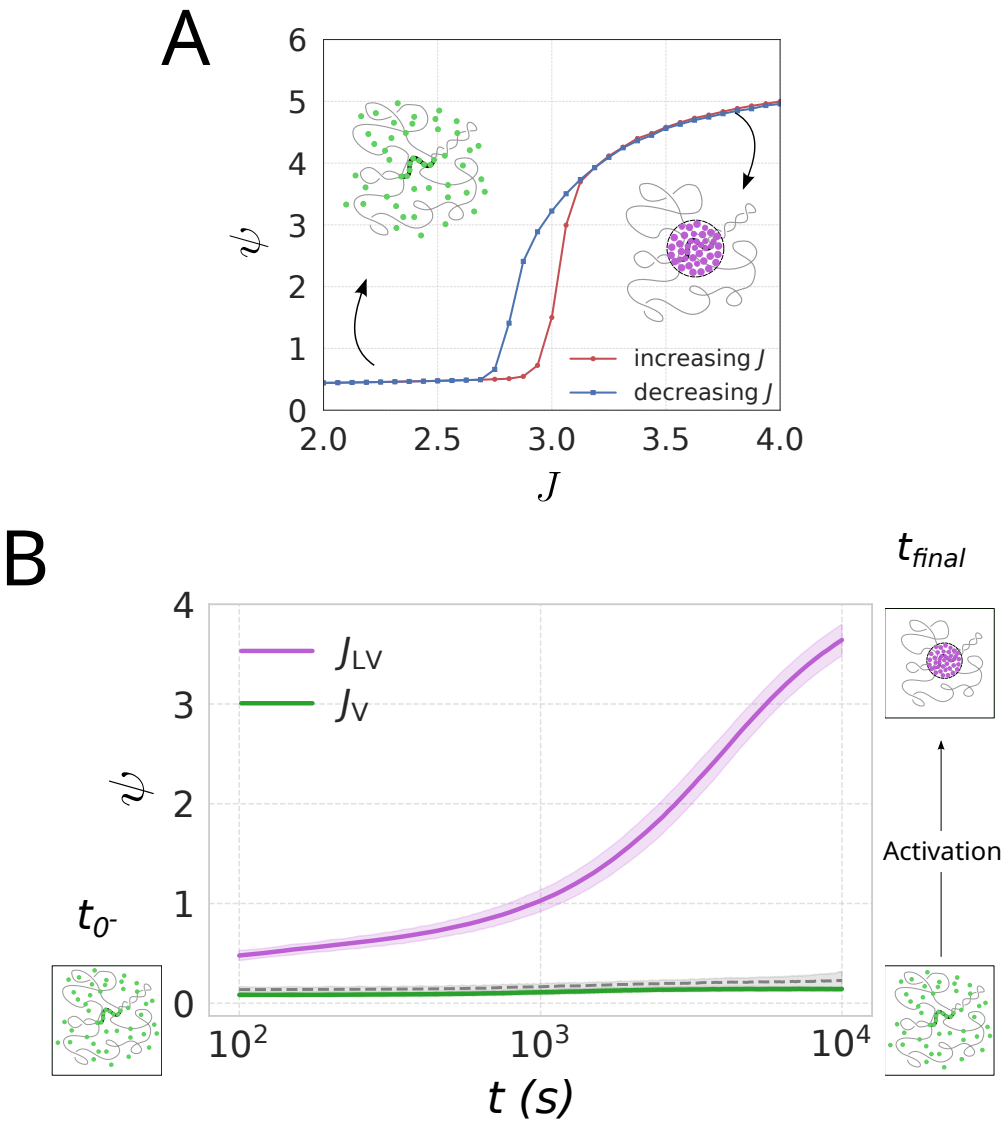

Figure 2. *Partition complex formation needs an activation in the LV phase.* **A** Equilibrium order parameter ψ as a function of the coupling constant J (expressed in unit of kT). The system, simulated on a $160\times40\times40$ lattice with $N_b = 300$ particles. The red and blue curves represent increasing and decreasing J, respectively. At low and high values of ψ, the system is in the vapor and liquid-vapor (LV) phases, respectively. Illustrations representing the system's state in each phase, using the same representation as Fig. 1. **B** Out-of-equilibrium order parameter versus time (same parameters as in panel A). The system, initially prepared in the vapor phase, relaxes towards equilibrium under two different conditions: vapor phase (green, $J = 2.5$) and activated (stable) LV phase (purple, $J = 4.7$). As a control, we plot in dashed grey an activation in the metastable region ($J = 3$).

(i) the absence of complex formation with $\Delta parS$ or some ParB variants, and (ii) the formation of a complex within the timescale of a fraction of the cell cycle with a functional ParABS system. In the next section, we present experimental evidence demonstrating that a complete ParB-CTP cycle is required for this phase transition and subsequent droplet formation.

3 A functional ParB-CTP cycle is essential for droplet formation

In this section, in support of our modeling, we demonstrate that modifications in the release of $\mathrm{ParB_F}$ from $parS_\mathrm{F}$ or in the clamped $\mathrm{ParB_F}$ unbinding hinder activation and thus droplet formation. For this, we investigated the ParABS_F system of plasmid F, focusing on mutations in the boxIII motif of the $parB_\mathrm{F}$ gene. Along with boxII, boxIII is involved in CTP binding and hydrolysis [16, 17]. This motif contains highly conserved asparagine (N) and arginine (R) residues (Fig. 3A). We generated two $\mathrm{ParB_F}$ variants by substituting these residues with alanine (A), resulting in $\mathrm{ParB_F}$-N153A and $\mathrm{ParB_F}$-R156A.

We started by analyzing the expression levels of these variants on mini-F plasmids (Fig. S1). $\mathrm{ParB_F}$-R156A exhibited expression levels comparable to wild-type (WT) ParB. ParA, the auto-repressor of the *par* operon stimulated by $\mathrm{ParB_F}$ bound to $parS_\mathrm{F}$ [28, 29], remained fully active, indicating that $\mathrm{ParB_F}$-R156A interacts normally with $\mathrm{ParA_F}$. In contrast, $\mathrm{ParB_F}$-N153A exhibited a fourfold overexpression, similar to plasmids lacking $parS_\mathrm{F}$, suggesting defects in partition complex assembly or $\mathrm{ParA_F}$-$\mathrm{ParB_F}$ interactions.

Next, using fluorescence microscopy, we investigated partition complex assembly. WT $\mathrm{ParB_F}$-mVenus formed bright and distinct foci in the presence of $parS_\mathrm{F}$ but not in the absence of $parS_\mathrm{F}$ (compare Fig. 3B(a) with 3B(b) [5]). The N153A variant showed diffuse fluorescence with no foci formation (Fig. 3B(c)), indicating a failure to assemble partition complexes. The R156A variant displayed an intermediate phenotype, with reduced foci intensity and increased background fluorescence (Fig. 3B(d)), suggesting partial defects in partition complex assembly.

To quantify these assembly defects, we performed a skewness analysis of fluorescence intensity distribution (Fig. 3B(e)). The skewness S measures the asymmetry in pixel intensity distribution relative to the intracellular average (See Supp. Methods). WT $\mathrm{ParB_F}$-mVenus exhibited high skewness ($S = 1.85$), reflecting the presence of bright foci, whereas the absence of $parS_\mathrm{F}$ (which prevents nucleation of foci), resulted in basal skewness ($S = 0.19$), consistent with diffuse fluorescence. The ParB-N153A and -R156A variants showed intermediate skewness values ($S = 0.57$ and 0.70, respectively), confirming impairments in partition complex assembly. We then performed a stability assay (See Supp. Methods) to evaluate whether these variants support effective plasmid partitioning. We measured the loss rate per generation of mini-F plasmids carrying the ParB-mVenus alleles. As previously reported, the mini-F with ParB-mVenus (WT) is highly stable, with a loss rate of 0.08%, while the $\Delta parS_\mathrm{F}$ counterpart is lost at a rate of 7.9% [5] (Table S1). The $parB_\mathrm{F}$-N153A and $parB_\mathrm{F}$-R156A alleles exhibited loss rates of 7.4% and 2.4%, respectively. These results confirm that the deficiencies in partition complexes assembly impair plasmid partitioning activity.

To further analyze the assembly defects, we performed ChIP-sequencing (ChIP-seq; Table S3), which quantifies ParB enrichment along the plasmid DNA [5, 8]. Enrichment at and near *parS* sites serves as a proxy for ParB droplet formation. In the absence of droplet formation, ParB enrichment is restricted to *parS* or its close vicinity, with a homogeneous non-specific distribution of ParB across the whole genome generates background noise in ChIP-seq profiles [8]. We focused on the right-hand side relative to *parS*, as enrichment decay spans larger genomic range, while the left-hand side is constrained by a roadblock as previously reported (Fig. S4) [5]. In Fig. 3C, the WT profile (black curve) shows ParB enrichment peaking at *parS*, followed by a rapid drop and long-range decay over $\sim$15 kb. As previous studied [5, 8], this decay is described by a power law obtained with the stochastic binding model, where ParB forms a droplet centered on *parS*. After normalization, the integral of the profile indicates ~ 120 ParB molecules in the enriched region, consistent with the estimated ~ 250 ParB dimers per complex [5] (with the remainder of ParB being likely bound to the chromosome). For the N153A variant (red curve), enrichment is observed exclusively at *parS*. Beyond *parS*, the profile immediately drops to basal levels, indicating that ParB is locked on *parS* and does not undergo the CTP-induced conformational change necessary to transition to the clamped form. The total ParB count, derived from the profile integral, is ~ 10, reflecting *parS*-bound ParB and residual nsDNA binding. This variant is thus unable to convert into the activated form required for recruiting additional ParB molecules to form droplets. In contrast, the R156A variant (blue curve) shows the drop after *parS* but does not reach basal levels, exhibiting a decay over 12 kb. The integral of this profile corresponds to ~ 30 ParB molecules. This residual decay likely arises from sliding clamps, consistent with the CS model where the release and unbinding parameter remain unchanged (Fig. S5 and analyses therein). While this mutation permits the formation of ParB clamps, it impairs their subsequent activation needed for recruiting additional ParB molecules. As a result, phase transition is prevented, though diffusion and unbinding are still observed.

We translate these findings into the framework of the CS model. For N153A (Fig. S6A), ChIP-seq and microscopy reveal no enrichment on nsDNA but only at *parS*, with no visible ParB droplets. Compared to

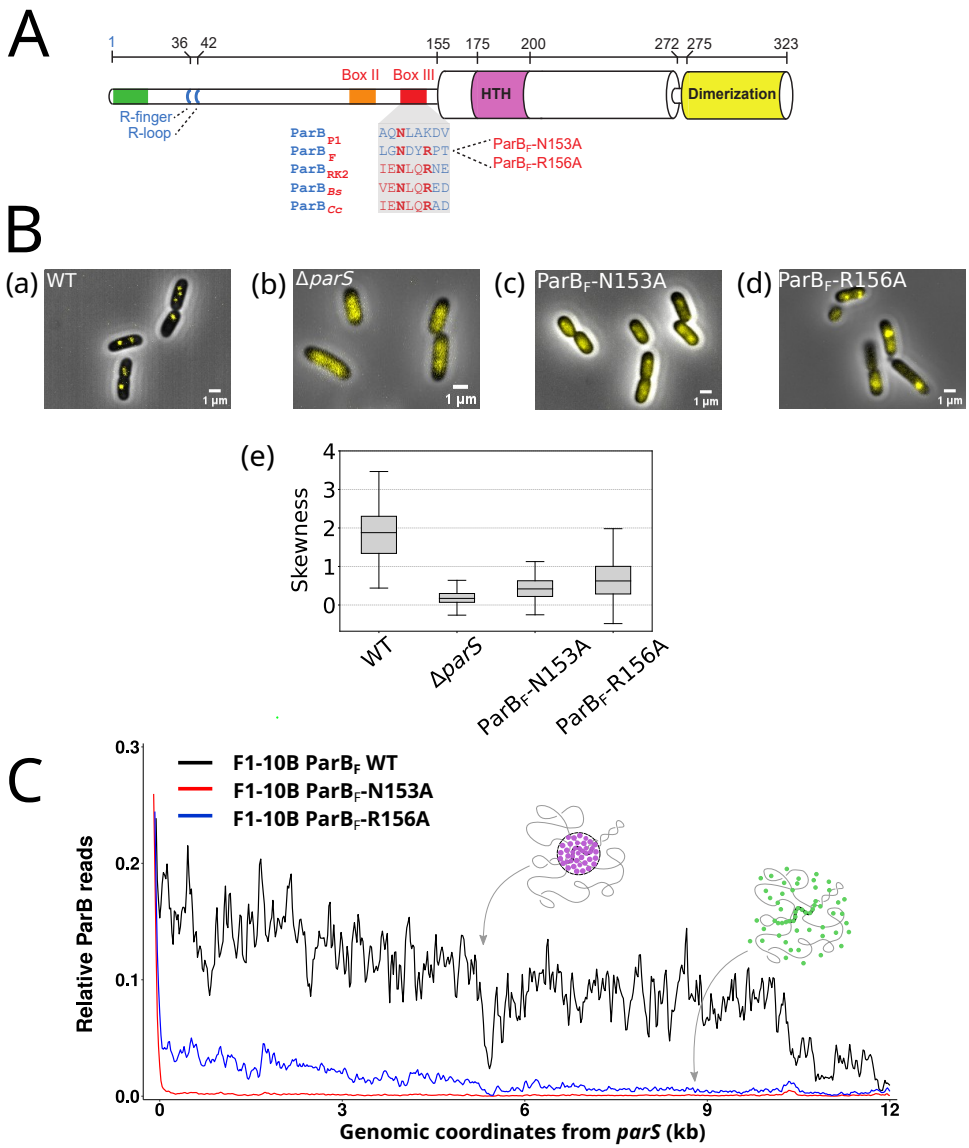

Figure 3. *The ParB-CTP cycle is essential for ParB droplet formation.* **A** Schematic representation of $ParB_F$. (Top) Amino acid (aa) numbering to scale. (Middle) Functional domains (Helix-Turn-Helix and dimerization) and motifs (Box II and III) are depicted. Thick cylinders (from aa 155–272 and 275–323) represent regions of $ParB_F$ resolved by X-ray crystallography, while thin cylinders (from aa 1–155 and 272–275) correspond to unresolved regions [27]. (Bottom) Conservation of the aa sequence in the BoxIII. Conserved residues from plasmids P1, F and RK2 and from the chromosomes of *Bacillus subtilis* (*Bs*) and *Caulobacter crescentus* (*Cc*) are colored in red. **B** Fluorescence imaging of $ParB_F$ fused with mVenus fluorescent tag *in vivo*. *E. coli* cells, grown in exponential phase, exhibit $ParB_F$-mVenus fluorescence expressed from the endogenous genetic locus of miniF plasmids. Representative images (a)-(d) and skewness analysis (e) of cells with miniF carying a deletion ($\Delta parS$) or not of *parS* and expressing $ParB_F$ WT or the variants $ParB_F$-N153A $ParB_F$-R156A. Scale bars: 1 μm . **C** The normalized average ParB reads are shown as a function of genomic coordinates from the right of *parS* over a 12.5 kb region for $ParB_F$ WT (black), $ParB_F$-N153A (green), and $ParB_F$-R156A (blue) variants. These profiles were determined by ChIP-sequencing from biological duplicates using *E. coli* cells carrying F1-10B derivatives. Additionally, an illustration of the resulting ParB macroscopic behavior from the model is provided, corresponding to Fig. 1A. Detailed ParB read distributions for each replicate, along with input data, are provided in Fig. S2-S4.

the WT model (described in Fig.3C), this corresponds to a new set of parameters where *parS* binding occurs normally at the rate B, but a modified release rate $R' = 0$ prevents the clamped form and activation switch, thereby inhibiting droplet formation. For ParB-R156A (Fig. S6B), ChIP-seq indicates residual enrichment consistent with CS (as modeled in Fig. S5) but not with droplet formation, supported by microscopy. This latter mutation likely impairs the activation switch required for ParB droplets formation but leaves other parameters unchanged.

These findings underscore the necessity of a fully functional ParB-CTP cycle for droplet formation, highlighting the role of ParB clamp activation in this process. The mutations studied here reveal distinct effects on ParB dynamics, demonstrating how disruption of either CTP binding and/or hydrolysis impairs LLPS and partition complex assembly.

Discussion

The partition complex exhibits liquid-like properties [10, 11], yet the mechanisms controlling ParB droplet formation remain incompletely understood. While the necessity of a functional *parS* site for droplet formation is well established [5, 8], the precise role of CTP in this process remains unclear. Recent studies have proposed the Clamping & Sliding (CS) model for partition complex assembly, which outlines a ParB-CTP cycle involving specific ParB binding to *parS*, followed by CTP binding, clamp formation, *parS*-release and CTP release-dependent hydrolysis DNA unbinding [12]. However, this model accounts for only a small fraction of ParB molecules (<10) bound to DNA, significantly fewer than the estimated ∼250 ParB molecules per partition complex [5]. Moreover, the CS model does not inherently rely on the liquid-like properties observed in ParB condensates. These discrepancies highlight the need to identify additional mechanisms, such as a CTP-dependent activation step of the ParB-ParB interactions during the CS cycle, to fully explain droplet formation. Reconciling the CS model with the liquid-like behavior of ParB droplets is therefore essential for understanding the assembly and function of the partition complex.

In this study, we propose that ParB activation for liquid-like behavior coincides with its transition into the clamped conformation. Evidence suggests that the synergistic effect of *parS* and CTP binding allows ParB to adopt a distinct conformational state [9, 17]. These *parS*-activated ParB-CTP forms persist after $parS_{\mathrm{F}}$ releases and enhances $\mathrm{ParB_F}$-$\mathrm{ParB_F}$ interactions, promoting DNA condensation through DNA-looping bridges [30]. This activation step serves as a critical switch, ensuring that ParB droplets form exclusively at *parS* sites, thereby preventing nonspecific aggregation elsewhere in the genome. Such precise localization is essential for maintaining cellular functionality and ensuring efficient DNA partitioning during the cell cycle. Our hypothesis is supported by both simulations and experimental evidence, which collectively highlight the central role of this activation step in coupling ParB droplet formation with its functional specificity.

To decipher the mechanisms of droplets formation, kinetic simulations using the LG model were employed to assess the timescale of this process. Knowing that droplets can only form in the LV phase, we initialized the system in the vapor phase and activated it to transition into the LV phase. Our simulations revealed that droplet formation occurs within a timescale corresponding to a fraction of the cell cycle. Our findings indicate that ParB cannot maintain a constant interaction energy (in the metastable region) to reproduce experimental observations, as previously proposed [10]. Instead, an additional mechanism is required to enhance ParB-ParB interactions in the presence of *parS*.

Our experimental results, using ParB variants in BoxIII impaired in the key steps of the CS cycle support this conclusion. For instance, the ParB-N153A variant, which fails to release from *parS*, likely due to deficient CTP binding (Fig. 3 and Ref. [9]), does not activate the ParB-ParB interactions necessary for droplet formation. Consequently, no droplets were observed, consistent with prior studies of variants that block the same step [8, 9], confirming the essential role of CTP binding in phase transition. Similarly, the ParB-R156A variant, which exhibits normal release from *parS* but reduced ParB binding to nsDNA near *parS*, appears locked in a conformation that prevents the transition required for phase separation (Fig. 3). The ParB profile for this variant corresponds almost perfectly with the prediction of the CS mechanism alone, lacking the activated ParB-ParB interactions (Fig. S5). These results can be interpreted within the framework of the CS model as follows: (i) ParB-N153A represents a system with no CTP-binding activation (R'=0), and (ii) ParB-R156A represents a clamped form locked in an inactive conformation. In both cases, the failure of ParB to switch to an activated form with enhanced $\mathrm{ParB_F}$-$\mathrm{ParB_F}$ interactions prevents droplet formation and partition complex assembly. These findings underscore the critical requirement not only for a fully functional CS cycle, but also for a finely tuned activation step during the ParB-CTP cycle to drive droplet formation and ensure efficient DNA partitioning.

In conclusion, we propose that CTP functions as a molecular switch, driving ParB from a vapor to a LV phase. The activation performed by coupling phase separation to ParB-CTP conformational changes ensures both the specificity and efficiency of ParB droplet formation at *parS*, preventing nonspecific aggregation elsewhere in the genome. To our knowledge, this represents the first identified switch mechanism regulating liquid droplet formation. Further investigations are needed to determine whether this switch can be directly triggered through ParB-ParB interactions upon

molecular contact. Understanding these interactions could provide broader insights into how CTP modulates phase transitions in cellular processes and partitioning mechanisms.

Acknowledgements

We thank G. Morla for its early involvement in the project during his master's studies. We also thank H. Sekkouri Alaoui for insightful discussions on the impairment of the two ParB variants. We acknowledge all members of the GeDy (CBI) and the SCPN (L2C) teams for fruitful discussions, and the staff at the GeT-Biopuces platform (INSA, Toulouse) for handling libraries and sequencing of ChIP-seq samples. This work was supported by the CNRS 80Prime MITI grant (ANCODS) and the ANR (BaDS; ANR-24-CE12-1319-01).

References

1. Stroberg, W. and Schnell, S. (2017) On the origin of non-membrane-bound organelles, and their physiological function. *Journal of Theoretical Biology,* **434**, 42–49.
2. Brangwynne, C. P., Eckmann, C. R., Courson, D. S., Rybarska, A., Hoege, C., Gharakhani, J., Jülicher, F., and Hyman, A. A. (Jun, 2009) Germline P granules are liquid droplets that localize by controlled dissolution/condensation. *Science,* **324**(5935), 1729–1732 Epub 2009 May 21.
3. Azaldegui, C. A., Vecchiarelli, A. G., and Biteen, J. S. (Apr, 2021) The emergence of phase separation as an organizing principle in bacteria. *Biophysical Journal,* **120**(7), 1123–1138.
4. Cornet, F., Blanchais, C., Dusfour-Castan, R., Meunier, A., Quèbre, V., Sekkouri Alaoui, H., Boudsoq, F., Campos, M., Crozat, E., Guynet, C., Pasta, F., Rousseau, P., Ton Hoang, B., and Bouet, J.-Y. (2023) DNA Segregation in Enterobacteria. *EcoSal Plus,* **11**, eesp–0038–2020.
5. Sanchez, A., Cattoni, D., Walter, J., Rech, J., Parmeggiani, A., Nollmann, M., and Bouet, J. (2015) Stochastic self-assembly of ParB proteins builds the bacterial DNA segregation apparatus. *Cell Systems,* **1**(2), 163–73.
6. Ah-Seng, Y. et al. (2009) Dual Role of DNA in Regulating ATP Hydrolysis by the SopA Partition Protein. *Journal of Biological Chemistry,* **284**(44), 30067–30075.
7. Davis, M., Martin, K., and Austin, S. (1992) Biochemical activities of the ParA partition protein of the P1 plasmid. *Molecular Microbiology,* **6**, 1141–1147.
8. Debaugny, R., Sanchez, A., Rech, J., Labourdette, D., Dorignac, J., Geniet, F., Palmeri, J., Parmeggiani, A., Boudsocq, F., Anton Leberre, V., and Walter, J. (2018) A conserved mechanism drives partition complex assembly on bacterial chromosomes and plasmids. *Molecular Systems Biology,* **14**(11), e8516.
9. Osorio-Valeriano, M., Altegoer, F., Das, C., Steinchen, W., Panis, G., Connolley, L., Giacomelli, G., Feddersen, H., Corrales-Guerrero, L., Giammarinaro, P., and Hanssmann, J. (2021) The CTPase activity of ParB determines the size and dynamics of prokaryotic DNA partition complexes. *Molecular Cell,* **81**(19), 3992–4007.
10. Guilhas, B., Walter, J.-C., Rech, J., David, G., Walliser, N.-O., Palmeri, J., and et al. (2020) ATP-driven separation of liquid phase condensates in bacteria. *Molecular Cell,* **79**(2), 293–303.
11. Babl, L., Giacomelli, G., Ramm, B., Gelmroth, A., Bramkamp, M., and Schwille, P. (2022) CTP-controlled liquid-liquid phase separation of ParB. *J Mol Biol,* **434**(2), 167401.
12. Walter, J.-C., Rech, J., Walliser, N.-O., Dorignac, J., Geniet, F., Palmeri, J., Parmeggiani, A., and Bouet, J.-Y. (2020) Physical Modeling of a Sliding Clamp Mechanism for the Spreading of ParB at Short Genomic Distance from Bacterial Centromere Sites. *iScience,* **23**(12).
13. Lin, D. C. and Grossman, A. D. (Mar, 1998) Identification and characterization of a bacterial chromosome partitioning site. *Cell,* **92**(5), 675–685.
14. Livny, J., Yamaichi, Y., and Waldor, M. K. (Dec, 2007) Distribution of centromere-like parS sites in bacteria: insights from comparative genomics. *Journal of Bacteriology,* **189**(23), 8693–8703.
15. Pillet, F., Sanchez, A., Lane, D., Anton Leberre, V., and Bouet, J.-Y. (2011) Centromere binding specificity in assembly of the F plasmid partition complex. *Nucleic Acids Research,* **39**(17), 7477–7486.
16. Osorio-Valeriano, M., Altegoer, F., Steinchen, W., Urban, S., Liu, Y., Bange, G., and Thanbichler, M. (2019) ParB-type DNA Segregation Proteins Are CTP-Dependent Molecular Switches. *Cell,* **179**(7), 1512–1524.e15 Copyright © 2019 Elsevier Inc. All rights reserved.
17. Soh, Y., Davidson, I., Zamuner, S., Basquin, J., Bock, F., Taschner, M., Veening, J., De Los Rios, P., Peters, J., and Gruber, S. (2019) Self-organization of parS centromeres by the ParB CTP hydrolase. *Science,* **366**(6469), 1129–33.
18. Jalal, A., Tran, N., and Le, T. (2020) ParB spreading on DNA requires cytidine triphosphate in vitro. *Elife,* **9**, e53515.
19. Connolley, L., Schnabel, L., Thanbichler, M., and Murray, S. M. (2023) Partition complex structure can arise from sliding and bridging of ParB dimers. *Nature Communications,* **14**(1), 4567.
20. Tišma, M., Janissen, R., Antar, H., Martin-Gonzalez, A., Barth, R., Beekman, T., van der Torre, J., Michieletto, D., Gruber, S., and Dekker, C. (2023) Dynamic ParB–DNA interactions initiate and maintain a partition condensate for bacterial chromosome segregation. *Nucleic Acids Research,* **51**, 11856–11875.
21. Erdmann, N., Petroff, T., and Funnell, B. (1999) Intracellular localization of P1 ParB protein depends on

ParA and parS. *Proceedings of the National Academy of Sciences of the United States of America,* **96**(26), 14905–14910.

22. Hirano, M., Mori, H., Onogi, T., et al. (Feb, 1998) Autoregulation of the partition genes of the mini-F plasmid and the intracellular localization of their products in Escherichia coli. *Molecular Genetics and Genomics,* **257**, 392–403.

23. Jalal, A., Tran, N., Stevenson, C., Chimthanawala, A., Badrinarayanan, A., Lawson, D., and Le, T. (2021) A CTP-dependent gating mechanism enables ParB spreading on DNA. *Elife,* **10**, e69676.

24. Bouet, J.-Y. and Funnell, B. E. (Jun, 2019) Plasmid Localization and Partition in Enterobacteriaceae. *EcoSal Plus,* **8**(2), 10.1128/ecosalplus.ESP–0003–2019 Epub 2019 Jun 12.

25. David, G. Structure et dynamique du cytoplasme auto-organisé : exemple par la ségrégation du génome bactérien PhD thesis (2019) Thèse de doctorat dirigée par Palmeri, John et Geniet, Frédéric Physique Montpellier 2019.

26. Le Gall, A., Cattoni, D., Guilhas, B., Mathieu-Demazière, C., Oudjedi, L., Fiche, J.-B., and et al. (2016) Bacterial partition complexes segregate within the volume of the nucleoid. *Nature Communications,* **7**(1), 12107.

27. Schumacher, M. A., Piro, K. M., and Xu, W. (Jun, 2010) Insight into F plasmid DNA segregation revealed by structures of SopB and SopB–DNA complexes. *Nucleic Acids Research,* **38**(13), 4514–4526.

28. Bouet, J.-Y. and Funnell, B. E. (1999) P1 ParA interacts with the P1 partition complex at *parS* and an ATP–ADP switch controls ParA activities. *The EMBO Journal,* **18**(5), 1415–1424.

29. Yates, P., Lane, D., and Biek, D. P. (Jul, 1999) The F plasmid centromere, sopC, is required for full repression of the sopAB operon. *Journal of Molecular Biology,* **290**(3), 627–638 Copyright 1999 Academic Press.

30. Taylor, J. A., Seol, Y., Budhathoki, J., Neuman, K. C., and Mizuuchi, K. (2021) CTP and parS coordinate ParB partition complex dynamics and ParA-ATPase activation for ParABS-mediated DNA partitioning. *eLife,* **10**, e65651.

31. Taylor, J. A., Pastrana, C. L., Butterer, A., Pernstich, C., Gwynn, E. J., Sobott, F., Moreno-Herrero, F., and Dillingham, M. S. (January, 2015) Specific and non-specific interactions of ParB with DNA: implications for chromosome segregation. *Nucleic Acids Research,* **43**(2), 719–731.

32. Sanchez, A., Rech, J., Gasc, C., and Bouet, J.-Y. (Jan, 2013) Insight into centromere-binding properties of ParB proteins: a secondary binding motif is essential for bacterial genome maintenance. *Nucleic Acids Research,* **41**(5), 3094–3103.

33. Diaz, R., Rech, J., and Bouet, J.-Y. (2015) Imaging centromere-based incompatibilities: Insights into the mechanism of incompatibility mediated by low-copy number plasmids. *Plasmid,* **80**, 54–62 ISPB Plasmid Biology Meeting 2014.

34. Diaz, R. E., Sanchez, A., Anton Le Berre, V., and Bouet, J.-Y. (2017) High-Resolution Chromatin Immunoprecipitation: ChIP-Sequencing. *Methods in Molecular Biology,* **1624**, 61–73.

35. Sekkouri Alaoui, H., Quèbre, V., Delimi, L., Rech, J., Debaugny-Diaz, R., Labourdette, D., Campos, M., Cornet, F., Walter, J., and Bouet, J. (Aug, 2024) In vivo assembly of bacterial partition condensates on circular supercoiled and linear DNA. *Molecular Microbiology,* Epub ahead of print.